Journal of
Advanced Civil and Environmental Engineering
Vol.5, No.2, 2022, pp 61-73
ISSN: 2599-3356
DOI: http://dx.doi.org/10.30659/jacee.5.2.61-73

Seismic Performance of Reinforced Concrete Bridge using Friction Pendulum Bearing Under Different Friction Coefficients

James Michael[1*], Muslinang Moestopo[1], Iswandi Imran[1,3], Dionysius M. Siringoringo[2], Erwin Lim[1], Shinsuke Yamazaki[4]

[1] *Civil Engineering Department, Institut Teknologi Bandung, Bandung, West Java, Indonesia*
[2] *Institute of Advanced Sciences, Yokohama National University, Yokohama, Japan*
[3] *Research Center for Disaster Mitigation, Institut Teknologi Bandung, Bandung, West Java, Indonesia*
[4] *Nippon Steel Engineering Co. Ltd., Tokyo, Japan*
**Corresponding author: j.michael@gmail.com*

(**Received:** 24th September 2022 ; **Revised:** 7th October 2022 ; **Accepted:** 30th October 2022)

Abstract: Application of seismic isolation system is important in bridges design, primarily in seismically active countries. Bridges are prone to damage from seismic forces. Elastomeric isolation bearings have been applied in short-span bridges for some time in most countries. These bearings are preferred because of the low maintenance cost. However, these bearings are not reliable when subjected to large displacement and low temperatures. In the other hand, friction sliding bearings shows better performance under the former circumstances despite its use is still limited to long-span bridges and has not been explored further. This paper describes a performance evaluation of seismically-isolated short-span reinforced concrete bridge using friction pendulum system (FPS). Seismic performances of non-isolated and isolated models from the reference bridge functioning as light rapid transit (LRT) bridge in Jakarta are investigated using nonlinear time history analysis. The results demonstrate that isolated bridges with FPS performed better than non-isolated bridges under 1000-year earthquake as shown by reductions of base shear force, absolute deck acceleration, and acceleration amplification ratio. Comparisons of isolated bridges with different FPS friction types and arrangement have demonstrated that the reference bridge with all Type A friction (μ_0 = 0.050) applied, performed the best among all other configurations.

Keywords: seismic isolation system; seismic force; friction pendulum system; seismic performance; nonlinear time history analysis; isolated bridge

1. Introduction

Seismic isolation is a design idea promoting separation of a whole or a part of structure or tools placed on a structure, to prevent damages induced by ground acceleration. Primary purpose of applying seismic isolator is for dissipating energy at the base of a structure, so that the acceleration at the superstructure can be reduced. As a simple structure, bridges have minimum resistance against earthquake forces (Kunde & Jangid, 2003). Application of base isolators at the pier heads can reduce lateral forces. Seismic isolation system works by shifting the primary natural period beyond the dominant period of the ground motion. Period shift is achieved by increasing lateral flexibility of the whole structure (Gimenez et al, 2018). Lateral seismic isolation bearings can be classified into elastomeric bearings and frictional sliding bearings (Naeim & Kelly, 1999).

Elastomeric bearings have been used to accommodate thermal expansion and rotation at bridge supports. These bearings have high tolerance for movement, overload, and minimal maintenance

requirements (Buckle et al, 2006). Lead rubber bearing is the most commonly used. It consists of dual steel plate cover, multiple elastomeric layers, and steel shims in between with a lead core. Elastomeric layers provide lateral flexibility and restoring force, lead core acts as energy dissipator, and steel shims provide vertical bearing capacity (Hameed et al, 2008). LRB is notable for having low maintenance costs (Kim and Yun, 2007). As a result, LRB has been a primary choice for seismic isolator in bridges during the last two decades in New Zealand, Japan, and the United States (Buckle and Mayes, 1990). However, elastomeric bearing size must be increased to maintain good stability when subjected to large displacement. This action will increase lateral stiffness of the isolator and render it ineffective. Furthermore, under low temperatures, crystallization of the rubber layers may occur and found to increase lateral stiffness of a LRB (Cardone et al, 2011). A study found that in the winter, LRB-isolated bridge pier ductility is reduced, and base shear is higher than in the other seasons (Billah and Todorov, 2019).

The frictional sliding bearings began to be developed in the late 1980s. There are two kinds of sliding bearings: flat sliding bearings, which applied as complement to elastomeric bearings, and friction pendulum bearings. The latter were introduced by Zayas et al in 1990. It consists of an articulated slider supported on a spherical concave surface. FPS are made from stainless steel plate with polytetrafluoroethylene (PTFE) coating. The device applies engineering principles of pendulum motion to shift the natural period of the structure away from the dominant period, in order to reduce impact of the seismic forces. Period shift can be achieved easily as it is only depended on the plate curvature radius. Excessive displacement may be prevented by applying adequate amount of friction damping on the sliding surface (Zayas et al, 1990). Application of FPS has some advantages such as eliminating torsional rotation of a bridge, distributing seismic forces uniformly, reducing three to four times seismically induced forces, and reducing equivalent linear stiffness of the whole structure (Dicleli and Mansour, 2002).

The application of FPS is still minimum compared to LRB in bridges design. In the United States, the usage of FPS in bridges is fewer than 5% of all isolated bridges constructed (Buckle et al, 2006). This may be due to the fact that the price of FPS is more expensive than any other seismic isolator devices (Ingham, 2003). Therefore, the usage of FPS is currently limited to long-span bridges with span length varied between 60 to 100 m, as can be observed of isolated bridges in various high intensity earthquake areas in China (Xia et al, 2015 and Mei et al, 2020).

This paper describes a study of the use of FPS for seismic isolation in a reinforced concrete bridge in Indonesia. The study includes design procedure of the seismic isolation system following the recent building and seismic codes. Bridge is observed and compared under condition of using isolation bearings and non-isolation bearings with finite element method. There are two main objectives of this study. The first objective is to compare the seismic performance of the conventional non-isolated bridge with FPS-isolated bridges under the same scenarios of ground motions using the recent building codes. The second objective is to determine the most optimum design of FPS by selecting friction type which exhibits most favorable responses. The paper is organized as such that the basic information on reference structures and isolation systems is explained first. Then, the design procedure of the isolation system is provided. Moreover, case study of finite element simulation of both non-isolated bridge and isolated bridges, is presented with discussion on the results. Finally, conclusions of the study will be provided.

2. Description of isolation system: Single concave friction pendulum (SCFP)

Isolator system used in this study is single concave friction pendulum (SCFP). The isolator unit consists of four main components: articulated slider, concave plate, sliding plate, housing plate, and sliding material. The sliding plate is attached to concave plate. All plate components are made from stainless steel. The housing plate are placed at the top of the articulated slider, whereas the sliding plate are placed on the bottom. The sliding material used is made from polytetrafluoroethylene (PTFE) and high strength fiber.

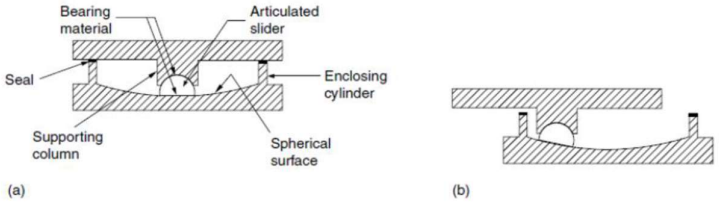

Fig. 1. Illustration of a SCFP bearing

Ground motion will act as lateral force, F, which will initiate movement of the slider when larger than the characteristic force of SCFP, Q_d. By considering $Q_d = \mu W$, the horizontal force equilibrium can be expressed as follows.

$$F = \frac{W}{R}u + \mu W \tag{1}$$

Note that the term of $\frac{W}{R}$ can be regarded as post-elastic lateral stiffness, thus natural period of the isolator can be expressed as the following equation:

$$T = 2\pi\sqrt{\frac{R}{g}} \tag{2}$$

Eq. 2 implies that the natural period of the SCFP only influenced by the radius of curvature of the concave plate. The idealized hysteretic loop of the isolator follows a bilinear model of characteristic force, $Q_d = \mu W$ and post-elastic lateral stiffness, $K_p = \frac{W}{R}$ (Fig. 2b)

(a) Free body diagram of SCFP (Courtesy of Roberto Villaverde) (b) Hysteretic loop of SCFP

Fig. 2. Single concave friction pendulum Isolator System

In this study, two types of SCFP bearings are used for the simulations. All bearings have the same radius of curvature of 4500 mm, and thus also have the same natural period of 4.26 s. But there are differences of bearing capacity and stiffness as can be seen on Table 1. The SCFPs are manufactured with two types of friction: Type A and Type B. Table 2 presents friction coefficient values of both types at different velocities and rate parameters of corresponding bearing pressure conditions.

Table 1. Type and specification of SCFP bearings used in the study

Model	Natural Period (sec)	Nominal Vertical Load (kN)	Post-elastic Horizontal Stiffness (kN/mm)	Ultimate Horizontal Displacement (mm)	Vertical Stiffness (kN/mm)	Effective Concave Plate diameter (mm)	Slider Diameter (mm)
NSSSB-40-200-410	4.26	1256	0.279	410	2500	1070	200
NSSSB-40-200-535	4.26	1256	0.279	535	2500	1320	200

Table 2. Friction coefficient of each type and bearing pressure

Friction Type	Bearing Pressure (σ) [MPa]	Friction Coefficient at maximum velocity (μ-fast)	Friction Coefficient at minimum velocity (μ-slow)	Rate Parameter (a) [s/mm]
Type A	40	0.050	0.030	0.008
Type B	40	0.046	0.025	0.017

Friction coefficient of the SCFP in general depends on velocity of the slider and can be expressed in the Equation 3.

$$\mu(v) = \mu_{fast} - \left(\mu_{fast} - \mu_{slow}\right) \times e^{-av} \tag{3}$$

3. Description of the design code and reference structure

Indonesia is situated between three tectonic plates namely, Pacific, Australian, and Sunda Block plates. Within 20 years, there are many cases of earthquake exceeding M_w 7.5 in Indonesia, namely, 2004 Great Sumatra (M_w 9.2), 2005 Nias (M_w 8.6), 2009 Padang (M_w 7.6), 2009 Papua (M_w 7.6), and the recent 2018 Palu-Koro (M_w 7.5) earthquakes. Fatalities are exceeding 200,000 in the 2004 Great Sumatra earthquake and the economic loss is quite enormous due to the destroyed infrastructures. Latest Indonesian seismic code for bridges used for this study, SNI 2833:2016, already included the updated seismic hazard map. The reference bridge is located in Jakarta city. Fig. 3 displays design acceleration response spectra of Jakarta for 1000-year return period with 5% damping assumption for soft soil type. Selected spectral parameters according to the Indonesian code are listed in Table 3. The analysis conducted in this study does not consider the effect of near-fault ground motion effect, as there is not known any active faults in Greater Jakarta area.

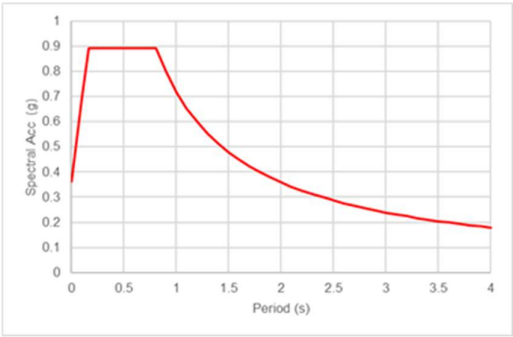

Fig. 3. Design acceleration response spectra of Jakarta city for the 1000-year return period

Table 3. Parameters for code design spectra used in the design of the reference bridges (Jakarta city, 1000-year earthquake) (SNI 2833:2016)

Site class	SE
Peak ground acceleration (PGA)	0.288 g
Seismic acceleration for 0.2 s period (S_S)	0.572 g
Seismic acceleration for 1 s period (S_1)	0.234 g
Amplification factor for PGA (F_{PGA})	1.26
Amplification factor for 0.2 s period (F_A)	1.556
Amplification factor for 1 s period (F_V)	3.064
Design peak ground acceleration (PGA_D)	0.363 g
Design acceleration for 0.2 s period (S_{DS})	0.89 g
Design acceleration for 1 s period (S_{D1})	0.717 g
Start period of constant acceleration (T_0)	0.161 s
End period of constant acceleration (T_S)	0.806 s

Reference structure observed in this study is light rapid transit (LRT) bridge consisting of 4 spans in total length of 100 m as shown in Fig. 4. The pier height varies between 7.3 and 8.2 m. The structure is constructed using reinforced concrete with compressive strength of 33 MPa and reinforcement bar of ASTM A615M Grade 60 with yield and ultimate strength of 413 MPa and 620 MPa, respectively.

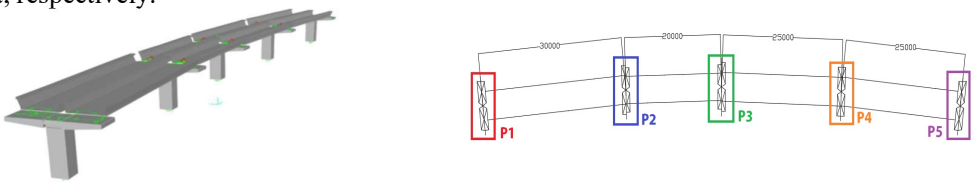

(a) Oblique view (b) Plan view

Fig. 4. The reference bridge

Six models have been analyzed in order to achieve better comprehension of impacts in application of SCFP in the reference bridge. Details of each model are presented in Table 4. Models EL and SS illustrate non-isolated bridges. Piers in Model EL are assumed to perform in an elastic behavior when subjected to 1000-year earthquake, while piers in Model SS are expected to perform in an inelastic behavior subjected to similar earthquake. Meanwhile, Models A, B, C, and D represent seismically isolated bridges with SCFP. Each pier will be applied with 8 units of SCFP bearing, in total of 40 units for the whole structure. Linear and nonlinear finite element analysis were conducted to the bridge models.

Table 4. Details on configurations of each model

Isolated models	
Model A	• P1, P2, P3, P4, P5: Type A, 40 MPa
Model B	• P1, P2, P4, P5: Type A, 40 MPa • P3: Type B, 40 MPa
Model C	• P1: Type A, 40 MPa • P2, P3, P4: Type B, 40 MPa • P5: Type A, 40 MPa
Model D	• P1, P2, P3, P4, P5: Type B, 40 MPa
Non-isolated models	
Model EL	Piers are assumed to have elastic behavior
Model SS	Piers are assumed to have inelastic behavior

4. Design procedures of the isolation systems

Preliminary design for the isolation bearings is involved with the vertical loads at each bridge pier. Maximum vertical loads in each pier are determined as a base to select suitable bearing. Moreover, in order to find the most optimum performance, the friction coefficient is also considered for each bearing type as shown in Table 5 i.e., Type A and Type B.

Simplified analysis method, as pointed by AASHTO GSID 2014, is used in this preliminary phase to predict the effective parameters of the isolation system. The analysis is conducted to determine whether the design displacement is exceeding the limitation. Effective stiffness (K_{eff}) of the isolator can be calculated by considering stiffness of the substructure (K_{sub}), characteristic force of the isolator (Q_d), and post-elastic stiffness of the isolator (K_{h2}), as can be seen in the Equation 4 and 5.

$$K_{eff} = K_{sub}\left(\frac{\alpha}{1+\alpha}\right) \tag{4}$$

$$\alpha = \frac{K_{h2}d+Q_d}{K_{sub}d-Q_d} \quad (5)$$

Once the effective stiffness is obtained, effective parameters such as period (T_{eff}), damping ratio (ξ), and isolator displacement (d_{iso}) can be calculated. The final isolator displacement should satisfy the acceptable limit. Otherwise, the bearing sizes have to be adjusted. Step-by-step analysis procedure is briefly explained in the following flowchart (Fig. 5). The total design displacement and effective damping are displayed in Table 5.

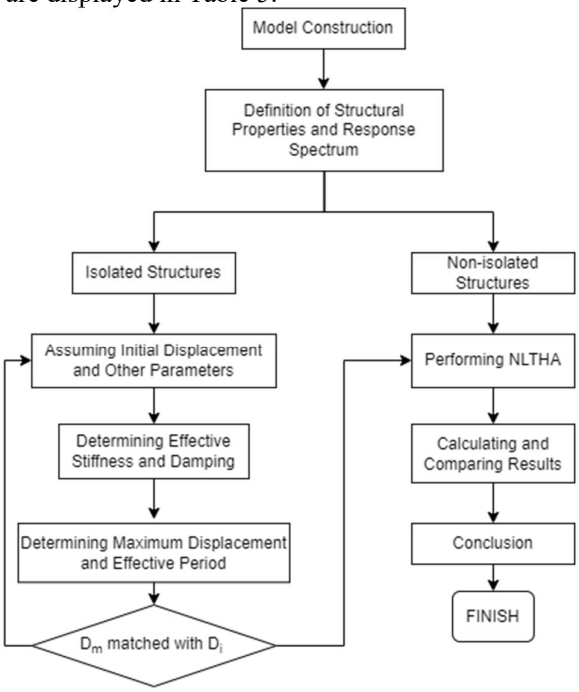

Fig. 5. Flowchart of the analysis procedure

Table 5. Design displacement and damping of isolated models

Parameter	Model A	Model B	Model C	Model D
Transversal Displacement (mm)	141.92	143.08	145.45	147.85
Longitudinal Displacement (mm)	142.76	143.90	146.26	148.64
Total Design Displacement (mm)	201.30	202.93	206.27	209.65
Effective Damping Ratio	34.7%	34.4%	33.9%	33.3%

Table 6. Effective natural period of isolated models

Model	Longitudinal (s)	Transversal (s)
A	1.701	1.639
B	1.724	1.654
C	1.751	1.684
D	1.758	1.692

For preventing excessive residual deformation, AASHTO GSID 2014 requires an isolation system to produce lateral restoring force difference, at total design displacement (TDD) and at half of the TDD, greater than 1.25% that of the superstructural weight. Table 7 shows that restorability of isolation system in all models is already fulfilled according to the requirements in AASHTO GSID 2014.

Table 7. Lateral restoring force capacity in isolated models

Parameter	Model A	Model B	Model C	Model D
Characteristic Strength (% of Weight)	5.03	4.95	4.78	4.62
TDD (Total Design Displacement) (mm)	201.30	202.93	206.27	209.65
Radius (mm)	4500	4500	4500	4500
Post-sliding stiffness (% of Weight/mm)	0.022	0.022	0.022	0.022
Restoring force at 0.5 TDD (% of Weight)	7.26	7.20	7.08	6.95
Restoring force at TDD (% of Weight)	9.50	9.46	9.37	9.28
Restoring force difference (% of Weight)	**2.24**	**2.25**	**2.29**	**2.33**
Minimum demand (% of Weight)	**1.25**	**1.25**	**1.25**	**1.25**
Status	**OK**	**OK**	**OK**	**OK**

5. Criteria for seismic performance evaluation

Bridge models in this study are simulated under seven pairs of ground motion record. In AASHTO GSID 2014, the average response may be used if there are seven pairs of record used. Indonesia has insufficient ground motion data, especially for case of Jakarta city. Therefore, the ground motion records were chosen as similar as possible to the most frequent earthquake mechanisms in Indonesia. Earthquake mechanisms used in this simulation are megathrust, shallow crustal, Benioff, and shallow background (Table 8). According to CALTRANS SDC 2.0 (2019), each ground motion pair shall be matched to the previously defined design spectrum with damping ratio of 5% (Fig. 6) and then be applied into minimum of 3 directions with 45-degree increment to find the maximum response thereafter. Matching period window was applied between 0.2T to 1.5T. Seismic responses were computed by using structural analysis software SAP2000. There are two basic criteria for performance used in this study: 1) evaluation based on the formation of plastic hinges on piers; 2) evaluation based on comparisons of base shear forces, isolator displacement, and absolute deck acceleration. All criteria were selected to determine the efficacy of the isolation system. In the first criterion, any possible plastic hinges formed were evaluated based on the classification in NCHRP 949. Performance criteria for the plastic hinge were defined following the compressive strain limit of the reinforced concrete column as shown in Table 9.

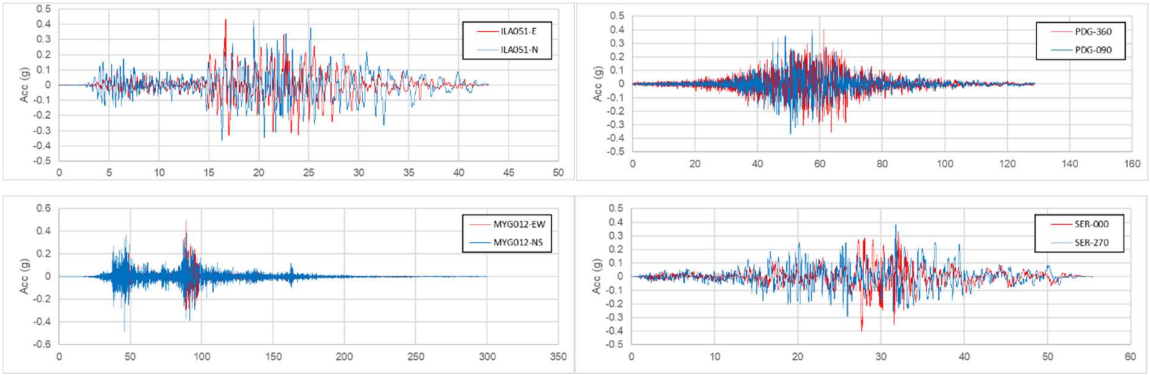

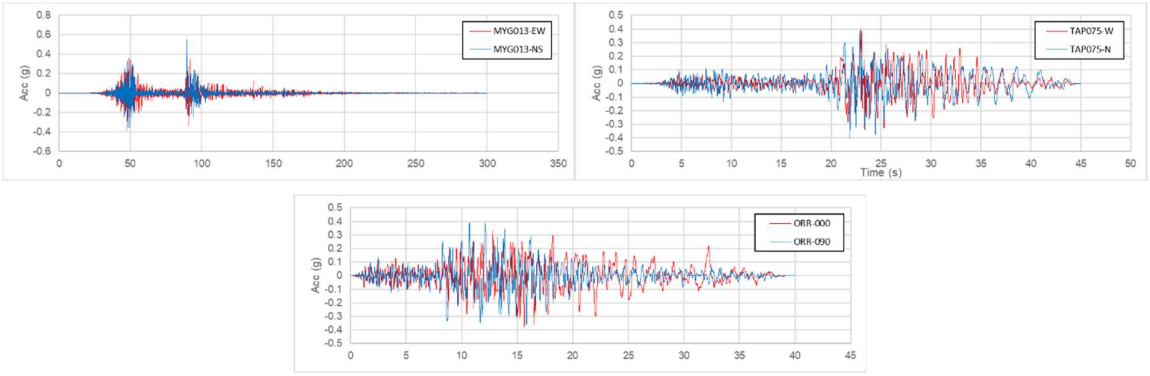

(a) Time history records

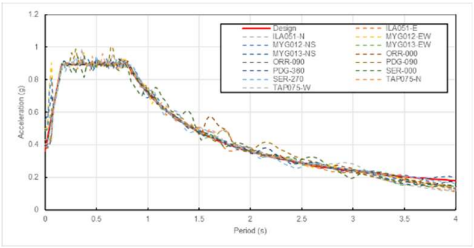

(b) Acceleration response spectra

Fig. 6. Spectra-matched historical ground motion records used for NLTHA

Table 8. Details on selected ground motion records

Mechanism	Code	Source	Earthquake	Magnitude (M_W)	Epicentral Distance (km)	Duration (s)
Megathrust	ILA051	PEER	Chi-Chi Earthquake 20 September 1999	7.62	160.21	43.00
	TAP075	PEER				45.00
	MYG012	K-NET	Tohoku Earhquake 11 March 2011	9.00	170.00	300.00
	MYG013	K-NET				300.00
Benioff	PDG	USGS	Padang Earthquake 30 September 2009	7.60	81.00	129.00
Shallow Background	ORR	PEER	Whittier Narrows Earthquake 10 January 1987	5.99	77.07	40.00
Shallow Crustal	SER	PEER	Landers Earthquake 29 June 1992	7.28	75.20	55.43

Table 9. Performance level of hinge defined in NCHRP 949

Performance Level (PL)	Description	Compressive Strain Limit
PL1	Life Safety	$\varepsilon_c = 1.4\left(0.004 + 1.4\frac{\rho_v f_{yh}\varepsilon_{su}}{f'_{cc}}\right)$
PL2	Operational	$\varepsilon_c = 0.004 + 1.4\frac{\rho_v f_{yh}\varepsilon_{su}}{f'_{cc}}$
PL3	Fully Operational	$\varepsilon_c \leq 0.004$

From the cross-sectional dimension, material, and reinforcement bar size, and the vertical load, a monotonic moment-curvature curve was obtained from calculation in XTRACT software. In order to construct a cyclic backbone curve according to NCHRP 949, several adjustments have been made to the monotonic curve. PEER/ATC 72-1 recommended to reduce the curve parameters as follow: 1) capping strength to be taken as 0.9 times of the monotonic curve, but not less than the yield strength, 2) pre-capping deformation to be taken as 0.7 times of the monotonic curve, 3) residual strength to be taken as 0.7 times of the monotonic curve. The cyclic backbone curve was assumed following Takeda hysteresis model, and assigned as nonlinear hinge to the base of each pier.

6. Analysis results and discussions

Effect on performance by isolating the bridge with SCFP was evaluated by acceptance criteria explained in the Section 5. By comparing the moment and rotation values of each pier, structural performance of each component was determined as fully operational (PL3), operational (PL2), or life safety (PL1). There were six piers evaluated in each finite element model. Fig. 7 shows piers that classified into operational level (PL2) in each model. Model EL is excluded from the evaluation, as they are assumed to have elastic behavior. The figure shows that all piers in conventional Model SS classified into operational level (PL2), thus condition in Model SS is classified as operational (PL2). Moreover, all isolated models (A – D) show no plastic hinges formed, thus the conditions are classified as fully operational (PL3). These results show that the performances of each isolated bridge are improved considerably compared to the conventional models.

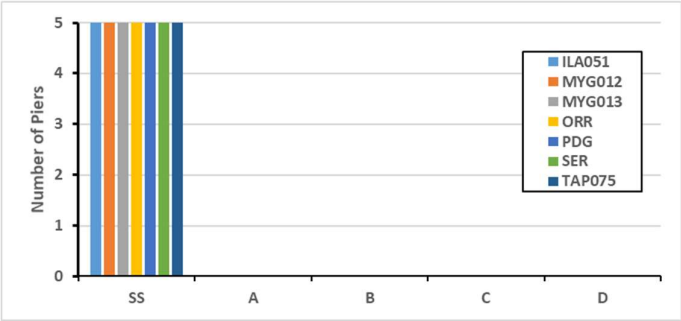

Fig. 7. Number of plastic hinges formed and the corresponding acceptance criteria from NLTHA of selected ground motion scenarios: piers in the reference bridge models with operational (PL2) criteria

Further evaluation in base shear force in all models (Fig. 8) showed that Model EL has the largest base shear forces in all ground motion scenarios. The result is understandable as Model EL is assumed to have elastic behavior. Model SS shows significant reduction of base shear, due to the inelastic behavior of the piers. As can be seen in the previous part, the reduction in Model SS followed by deterioration of structural performance. However, isolated models (A – D) show smaller base shear forces than the conventional ones. This may be due to the period shifting occurs

at the isolator level, thus reducing input acceleration to the structure. Note that base shear forces between each isolated model have high similarity in value, indicating that there is little influence of friction coefficient difference on the base shear force.

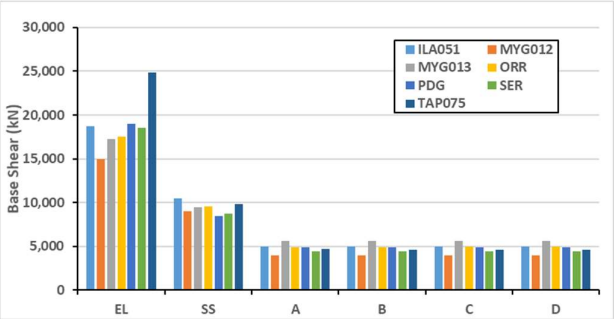

Fig. 8. Base shear forces of respective bridge models

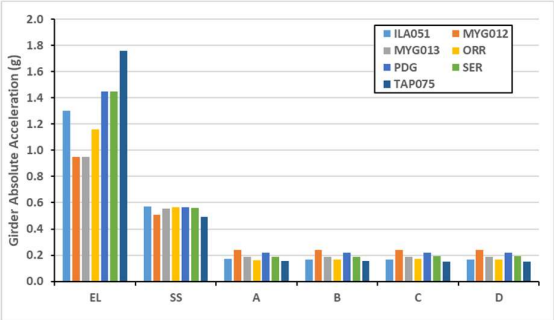

Fig. 9. Absolute deck accelerations in respective bridge models

Fig. 9 reveals absolute acceleration at deck level in all models analyzed. Note that acceleration values in isolated Models A – D are much lower than the conventional models. It becomes evident that SCFP isolation system is effective in reducing the absolute acceleration at deck level. However, it should be noted that the absolute acceleration has minor difference in each isolated model. Therefore, it is implied that friction coefficient variation does not have much influence on bridge absolute deck acceleration.

Peak isolator displacements in all isolated models are displayed in Table 10. Ultimate lateral deformation limit of the bearing is 410 mm. By applying safety reduction factor (α = 0.75), allowable isolator deformation is 307.5 mm. Safety factor of the isolation system is determined by dividing the peak isolator displacement value with the allowable deformation. The system is assumed to be safe if it has safety factor of larger than 1.0. Therefore, it can be concluded that isolation systems of all isolated models are within acceptable limit. Moreover, it should be noted that Model A has the largest safety factor of 1.326.

Table 10. Peak isolator displacement in isolated bridge models

Load Case	Model			
	A	**B**	**C**	**D**
ILA051	199.92	210.82	207.15	206.72
MYG012	230.90	239.07	248.94	248.76
MYG013	227.31	232.01	231.92	231.59
ORR	181.14	191.81	192.66	191.31
PDG	289.07	297.17	298.91	298.78
SER	244.94	256.65	262.95	262.33
TAP075	250.30	262.80	259.19	258.67
Average	**231.94**	**241.48**	**243.10**	**242.59**
SF	**1.326**	**1.273**	**1.265**	**1.268**

Fig. 10 shows the comparison of isolator hysteresis curves in observed isolated models, obtained from nonlinear time history analysis. By observing hysteresis curves in both directions, isolators in all models still fall within the force and deformation limits.

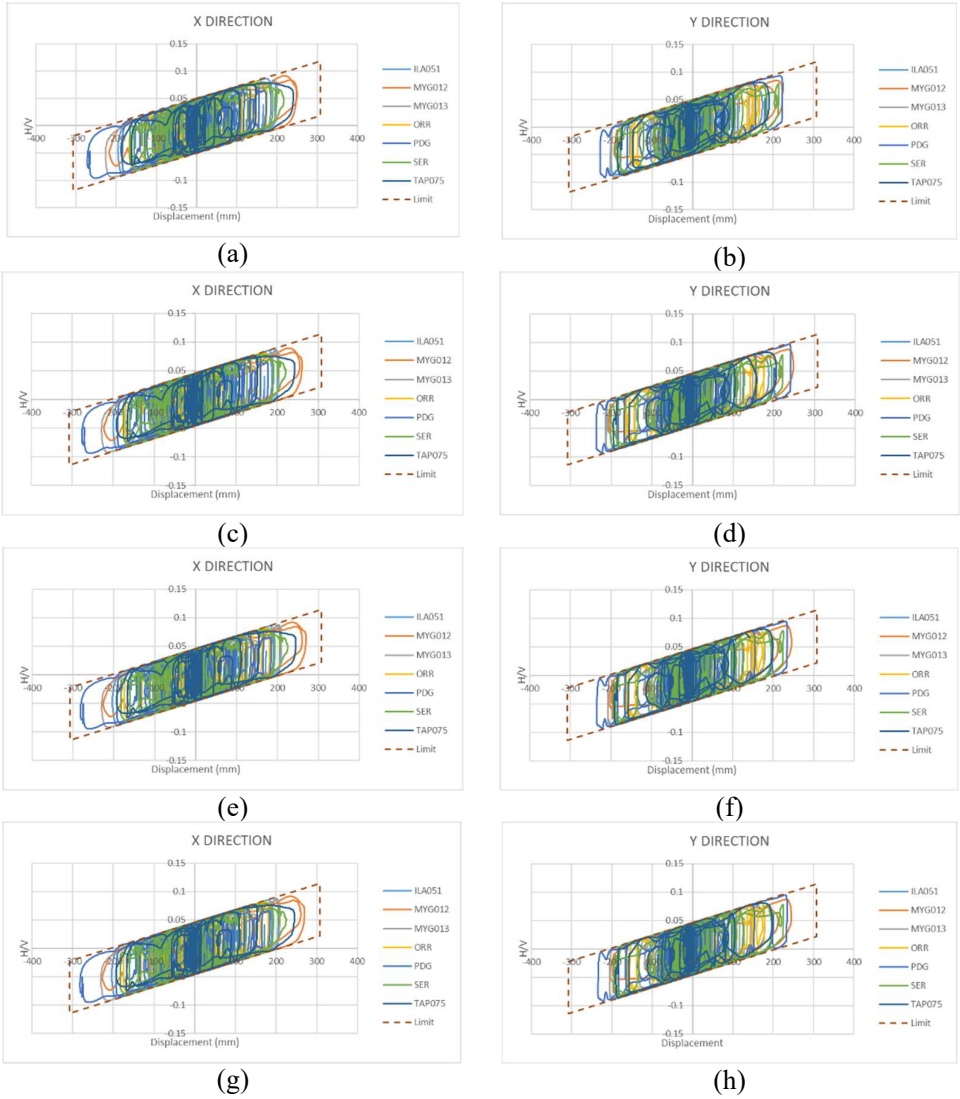

Fig. 10. Isolator hysteretic curves of isolated bridge: (a,b) Model A, (c,d) Model B, (e,f) Model C, (g,h) Model D

Next, sensitivity analysis was conducted to determine how the input variables impact the output parameters. In this study, the observed input variable is friction coefficient of the isolator and the output parameters are base shear force, absolute deck acceleration, and isolator displacement. The data was processed by conducting Min-Max Normalization procedure and linear regression. Variables and parameters from all models were scaled according to Equation 6.

$$NX = \frac{X - X_{min}}{X_{max} - X_{min}} \tag{6}$$

Fig. 11 shows that normalized displacement trendline have steeper slope than other output parameters. Thus, it can be conceded that isolator displacement is particularly more sensitive than other output parameters, to the friction coefficient changes. Insensitivity of base shear force and acceleration are not surprising, as there are little differences of natural period as presented in

Table 6, which causing similar input forces in isolated models. Moreover, if the input forces are assumed to be similar, the sensitivity of displacement are expected to follow the relation in Equation 1.

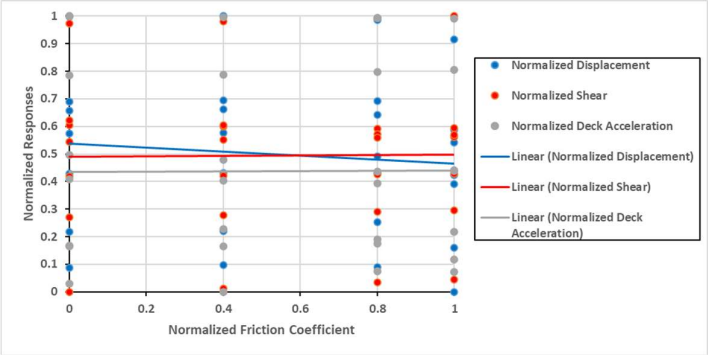

Fig. 11. Sensitivity analysis of observed parameters in the isolated bridge

7. Conclusions

This paper has described a case study of performance evaluation and optimization of seismically isolated concrete bridges using single-concave friction pendulum (SCFP) bearings. Structural design procedure and evaluation has been carried out using nonlinear finite element analysis in two different reinforced concrete bridge models under 1000-year earthquake. The study compared performance of the isolated bridges to the conventional non-isolated bridges and presented design optimization by using SCFP bearing with different friction types and arrangements.

After conducting the finite element analysis and observation on the structural responses, the study can be concluded as follows.

1. Seismically isolated bridge with SCFP bearing have better performance compared to the conventional bridge under the same 1000-year earthquake simulated in Jakarta city. As compared to the elastic design, the conventional models show reductions of: 1) base shear forces at 49.9%; and 2) absolute deck accelerations at 57.6%. On the other hand, improvements in isolated models include the average reduction of: 1) base shear forces at 74.4%; and 2) absolute deck accelerations at 85.3%. Moreover, restoring forces of the SCFP still satisfies the required demand.
2. Results show that under 1000-year earthquake, all piers are classified into operational level (PL2) in the conventional model. On the other hand, no plastic hinges are detected at all piers in isolated models, thus can be classified into fully operational level (PL3). Therefore, it can be concluded that overall performance level of each isolated bridge model is improved.
3. Results show that total application of Type A bearings ($\mu_0 = 0.050$) in the reference bridge, as in Model A, display the highest safety factor of isolator deformation among all other arrangements at 1.326.

References

[1] American Association of State Highway and Transportation Officials. (2012). *AASHTO LRFD Bridge Design Specifications: Customary U.S. Units.* Washington, D.C: AASHTO

[2] American Association of State Highway and Transportation Officials. (2014). *AASHTO Guide Specifications for Seismic Isolation Design 4th Edition*. Washington, D.C: AASHTO

[3] Billah, A.H.M.M. & Todorov, B. (2019). "*Effects of Subfreezing Temperature on The Seismic Response of Lead Rubber Bearing Isolated Bridge*". Soil Dynamics and Earthquake Engineering Vol. 126, 1-13

[4] Buckle, I.G. & Mayes, R.L. (1990). "*Seismic Isolation: History, Application, and Performance – A World View*". Earthquake Spectra Vol. 6(2), 161-201
[5] Buckle, I., Constantinou, M., Dicleli, M., & Ghasemi, H. (2006). "*Seismic Isolation of Highway Bridges"*. Buffalo: MCEER, University at Buffalo, The State University of New York
[6] California Department of Transportation. (2019). "*CALTRANS Seismic Design Criteria Version 2.0"*.
[7] Cardone, D., Gesualdi, G., & Nigro, D. (2011). "*Effects of Air Temperature on The Cyclic Behavior of Elastomeric Seismic Isolators*". Bull Earthquake Engineering Vol. 9, 1227-1255
[8] Dicleli, M. & Mansour, M.Y. (2003). "Seismic Retrofitting of Highway Bridges in Illinois Using Friction Pendulum Seismic Isolation Bearings and Modelling Procedures". Engineering Structures Vol. 25 (9), 1139-1156
[9] Gimenez, J. L., Himeno, T., Yoshihara, S., & Nurruzaman, A. S. M. (2018). "*Seismic Isolation of Bridges: Devices, Common Practices in Japan, and Examples of Application*". 4th International Conference on Advances in Civil Engineering 2018, Chittagong, Bangladesh, 1-6
[10] Hameed, A., Koo, M. S., Do, T. D., & Jeong, J. H. (2007). "*Effect of Lead Rubber Bearing Characteristics on The Response of Seismic-Isolated Bridges*". KSCE Journal of Civil Engineering Vol. 12 (3), 187-196
[11] Ingham, T.J. (2003). "*Nonlinear Time History Analysis of The Million Dollar Bridge*". Computational Fluid and Solid Mechanics 2003, 343-346
[12] Kim, Y.S. & Yun, C.B. (2007). "Seismic Response Characteristics of Bridges Using Double Concave Friction Pendulum Bearings with Tri-linear Behavior". Engineering Structures Vol. 29 (11), 3082-3093
[13] Kunde, M.C. & Jangid, R.S. (2003). "*Seismic Behavior of Isolated Bridges: A-State-of-The-Art Review*". Electronic Journal of Structural Engineering Vol. 3, 140-170
[14] Mei, K.H., Fu, W.W, Su, J.F. (2020). "Seismic Analysis of Hybrid System Bridge of Multi-Span Continuous Girder and Arches". E3S Web of Conferences 165 CAES 2020, 1-6
[15] Ministry of Public Works and Housing (Indonesia). (2017). *Earthquake Hazard Map for Bridges 2017*. Website: http://lini.binamarga.pu.go.id (Accessed 10 July 2021)
[16] Naeim, F. & Kelly, J.M. (1999). *Design of Seismic Isolated Structures From Theory to Practice*. Toronto: John Wiley & Sons, Inc.
[17] National Academies of Sciences, Engineering, and Medicine. (2020). *NCHRP 949: Proposed AASHTO Guidelines for Performance-Based Seismic Bridge Design*. Washington, DC: The National Academies Press
[18] National Standardization Agency of Indonesia. (2016). *SNI 2833:2016, Perencanaan Jembatan Terhadap Beban Gempa*. Jakarta: BSN
[19] Pacific Earthquake Engineering Research Center & Applied Technology Council. (2010). *PEER/ATC 72-1: Modeling and Acceptance Criteria for Seismic Design and Analysis of Tall Buildings*. Redwood City: ATC
[20] Villaverde, R. (2009). *Fundamental of Earthquake Engineering*. Boca Raton: CRC Press
[21] Xia, X.S., Cui, L.B., Chen, X.C. (2015). "Seismic Isolation of Long Span and Super Long Unit Continuous Beam Bridge with Friction Pendulum Bearings". Engineering Mechanics Vol. 32, 167-171
[22] Zayas, V. A., Low, S. S., & Mahin, S. A. (1990). "*A Simple Pendulum Technique for Achieving Seismic Isolation*". Earthquake Spectra Vol. 6 (2), 317-333